ULTIMATE CAPACITY IN TERMS OF ENERGY OF WAFFLE-FLAT-PLATE STRUCTURES SUBJECTED TO BIDIRECTIONAL SEISMIC LOADINGS

J. Donaire-Ávila[1], D. Galé-Lamuela[2], A. Benavent-Climent[3]

[1] *Assistant Professor, University of Jaén, Spain, jdonaire@ujaen.es*
[2] *PhD. Student, Technical University of Madrid, Spain, david.gale@upm.es*
[3] *Professor, Technical University of Madrid, Spain, amadeo.benavent@upm.es*

Abstract

This study investigates the ultimate capacity, in terms of input energy E_I expressed as equivalent velocity V_E, of waffle-flat-plate (WFP) structures subjected to biaxial seismic actions. First, the results obtained from shake-table testing carried out on a WFP specimen subjected to biaxial seismic loads are briefly presented. The specimen was subjected to the two horizontal components of the ground motion recorded during the Campano-Lucano earthquake (Italy, 1980) at Calitri station (C). The loading was applied in successive seismic simulations of increasing intensity until the collapse of the structure. Next, a numerical model was developed and calibrated with the experimental results. This model was, in turn, subjected to a set of ordinary records (without pulses). Each pair of records was applied in a sequence of scaled seismic simulations until failure. The ultimate state was assumed to be reached when the specimen or the numerical model experienced large lateral displacements. The ultimate values of V_E in the X and Y directions, V_{Ex} and V_{Ey}, obtained for the test specimen and for the numerical model are presented. Furthermore, a simple model is tentatively proposed to characterize the ultimate capacity of the structure in terms of energy, under biaxial seismic actions.

Keywords: bidirectional seismic loadings, input energy, waffle-flat-plate

1. Introduction

The seismic capacity of structures is usually established through two independent analyses in two (orthogonal) horizontal directions. Then, the maximum values of forces and displacements are obtained by applying combination rules such as the square root of the sum of the squares (SRSS) or its linear approximation in proportion 1:0.30 [1]. Eurocode 8 Part 1 applies this procedure to both the force-based methodology represented by the modal response spectrum analysis and the non-linear static analysis (pushover). Further methodologies such as displacement-based design [2,3] or energy-based design [4] estimate the capacity of the structure by analyzing two planar models.

Most studies on the seismic capacity of RC structures under bidirectional seismic loadings are related to isolated structural elements, mainly columns. The interaction of biaxial bending moment with axial force [5] and stiffness degradation [6,7] are topics deeply studied for columns. The capacity of columns subjected to bidirectional cyclic loadings has been also studied, especially through interaction curves for strength and displacements. De Stefano and Faella [8] proposed a yield condition for two degree-of-freedom models subjected to bidirectional loadings represented by an elliptical domain for both strengths and displacements. Bousias et al. [5] tested columns under biaxial loading and proposed an ultimate elliptical domain for the chord rotation from one obtained under uniaxial loadings along the two main axes. Fardis [9] proposed a similar expression for yielding. The capacity of columns in terms of dissipated energy has been also studied. Columns subjected to bidirectional loadings with constant axial load lead to levels of dissipated energy higher than under uniaxial load [6,8]. Nevertheless, this is not so evident when the axial load is not constant [7], which is the case for example of corner columns. Because the evolution of damage in columns subjected to bidirectional loadings is an important issue, indexes capable of tracking this damage have been proposed in the literature [10]. The hysteretic behavior is also affected by biaxial loading; for columns, the hysteretic and softening properties are different under bidirectional and under uniaxial loading.

The response of the complete structure under biaxial cyclic loadings cannot be assessed as a simple extension of the response under uniaxial loadings. Furthermore, the results obtained for isolated columns cannot be simply extrapolated to the whole structure. Magliulo and Ramasco [11] compared the response of a RC multistory frame building under unidirectional and under bidirectional seismic loadings, and showed that even though base shear and top displacements were similar, there were significant differences in terms of plastic deformation demands in columns. In contrast to uniaxial loading, there is a critical incidence angle of bidirectional seismic loading that produces the maximum response of the structure [12]. De Stefano and Faella [8] investigated one-story systems subjected to two-components of the earthquake (torsional effects not considered) and found that the hysteretic energy demand tends to concentrate in the stiff direction —lower period— and that this damage concentration is particularly significant for short periods. These authors proposed an overstrength in that direction (between 20% and 40%) for offsetting the increase of the expected damage with respect to that under unidirectional loading. In terms of displacements, a considerable increase is observed in systems subjected to bidirectional loadings with respect to unidirectional loads [13].

The influence of spatial effects derived from the torsional effects is also a critical issue in structures under bidirectional loadings, even for symmetric structures that undergo plastic deformations. Goel [14] found that symmetric and asymmetric structures have a similar demand for input and hysteretic energy; but the distribution of energy in asymmetric structures can be significantly different, with higher demand in flexible frames (closer to the mass center) than that in stiff frames (farther from the mass center). Moreover, the change of stiffness in one direction can affect the structural behavior notably in the orthogonal direction, which in turn depends on the characteristics of the ground motions.

Most of the experimental research on structures subjected to bidirectional loadings is based on pseudostatic tests, whereas studies based on shake-table dynamic tests are scarce [15,16]. This paper addresses seismic capacity in terms of energy of waffle-flat-plate structures subjected to bidirectional seismic loadings. Firstly, a numerical model that represents a portion of a 3-story waffle-flat-plate structure with an irregular layout of columns was developed and validated —the benchmark numerical model— through the results obtained in a shake-table test. Secondly, different sets of pairs of ground motion records were selected and applied in a sequence of scaled seismic simulations to the numerical model until collapse. Eventually, the total input energy and the energy dissipated through plastic deformations up to collapse was obtained and is discussed.

2. Benchmark numerical model and validation

2.1 Shake-table tests

First, a 3-story prototype structure consisting of waffle-flat-plates supported on isolated columns with an irregular layout was designed. The structure corresponds to a residential building located in Granada —a low-to-moderate seismicity region of Spain— and designed according to current Spanish standards. From the prototype, a portion formed by one exterior and two interior columns comprising one and a half stories — ground floor and first story— was selected and scaled by 2/5 (Fig.1). The ends of the columns of the upper story were pinned to reproduce null bending moment conditions at mid-height of the columns under lateral load. Steel plates were placed above the columns to simulate the gravity loads and to satisfy similitude laws. The scaled portion of the prototype structure was built in laboratory and instrumented with accelerometers, displacement transducers (LVDTs and lasers) and strain gauges. Fig.2 offers details of the geometry and reinforcement of the structural members. For columns, S-0, S-1 and S-2 respectively correspond to the sections at the lower part of the columns (foundation), at the upper part of the columns in the ground floor (below the plate), and at the lower part of the columns in the first floor (above the plate).

2

2i-0038
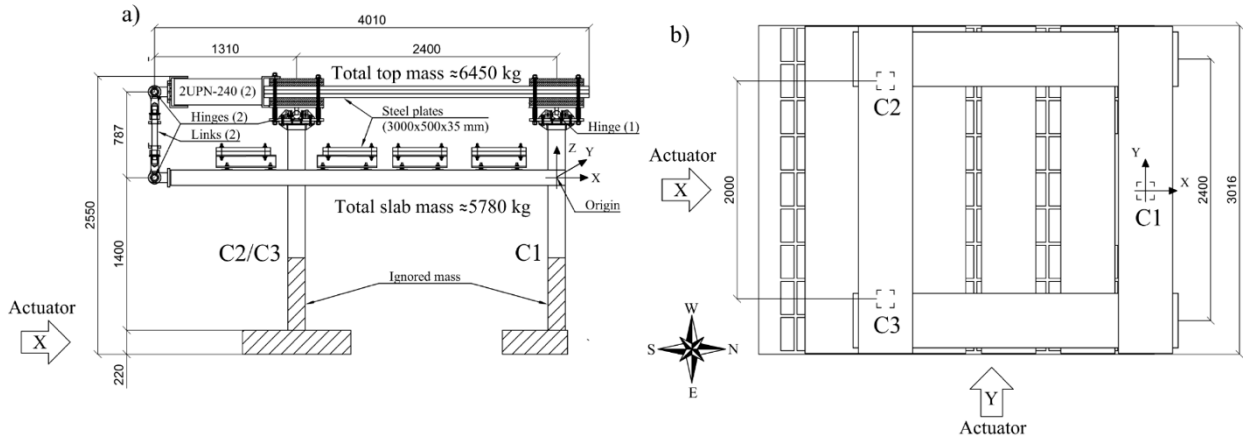
Fig. 1 – Specimen of waffle-flat-plate structure: (a) view in elevation; (b) view in plan
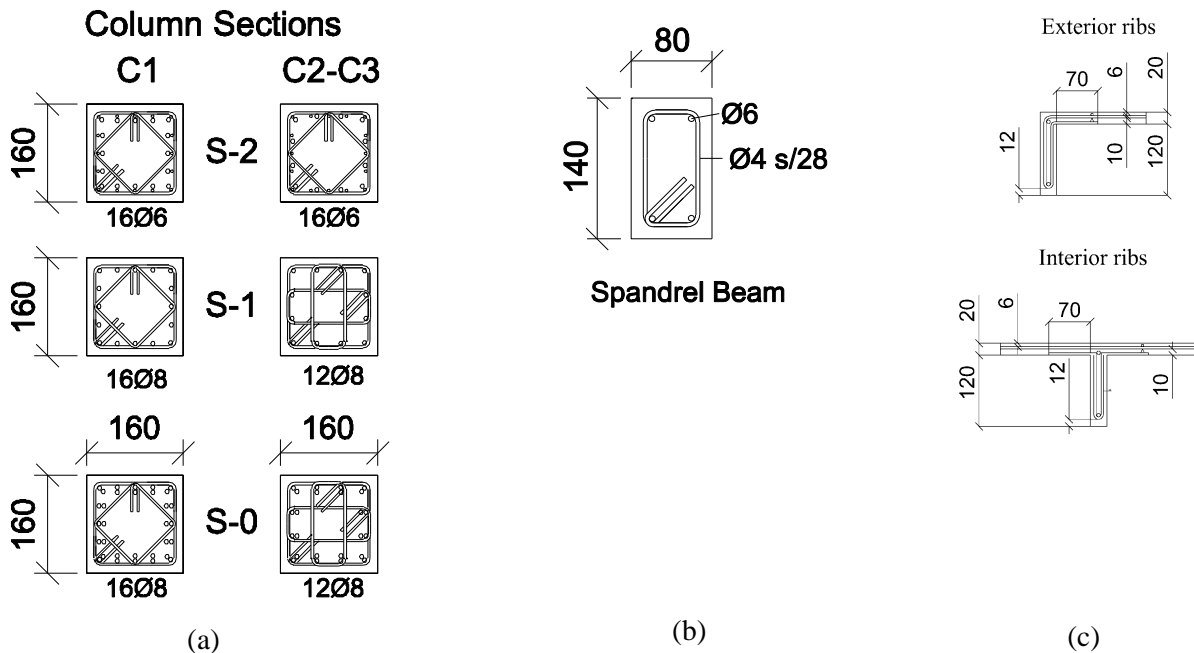
Fig. 2 – Geometry and reinforcement of columns (a), transverse beam (b) and ribs of the plate (c)

The specimen was set up on a shake-table equipped with two horizontal actuators (Fig.3) and subjected to bidirectional simulations until collapse using the two horizontal components of the ground motion registered at the Calitri station during the Lucano-Campano earthquake (Italy, 1980). The peak ground acceleration, *PGA*, of the original records was scaled to 35%, 50%, 100%, 200% (partial), 200% (full) and 300% (hereafter identified as C35, C50, C100, C200i, C200 and C300, respectively) in order to produce increasing levels of the seismic action. Before applying this sequence of seismic simulations, the specimen was subjected to a short-pulse vibration during the training phase, named T10. Response in terms of forces, displacements and energies obtained from the test are explained in detail in reference [15].

3
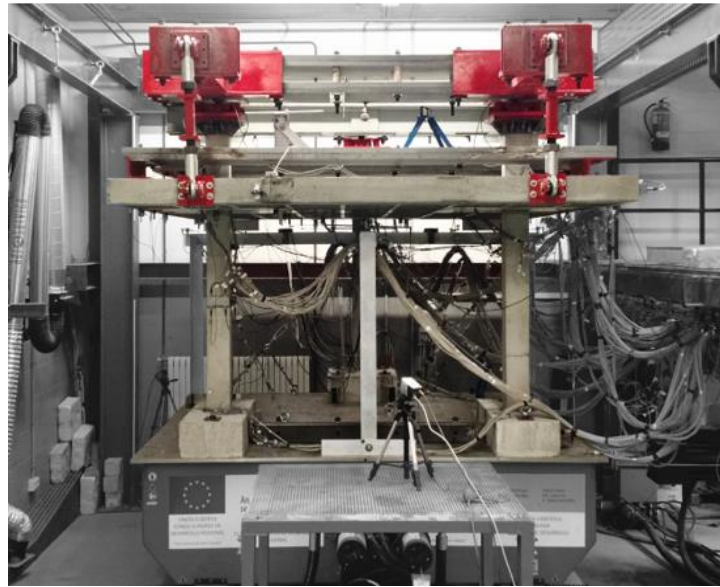
Fig. 3 – View of the specimen installed on the shake-table equipped with two actuators

2.2 Benchmark numerical model

A 3-D numerical model that represented the tested specimen —benchmark numerical model— was built in OpenSees [17]. The model is made up of 1802 nodes and 1810 elements. Columns proved to be the critical elements in the numerical model, since they exhibited the largest non-linear behavior during tests and governed the overall response of the structure. RC columns were modeled using non-linear frame elements. Concrete compressive strength was 44 MPa and the yield strength of the steel rebars 545 MPa, with a strain-hardening ratio of 0.003. The non-linear behavior is formulated according to the *Modification of Two-Point Gauss–Radau Integration*, for which the frame element comprises three parts: the two end parts are lumped plastic hinges, while the central part uses fiber elements. The length of the end parts is determined by the plastic hinge length, l_p, which is taken here as the depth of the transverse section, i.e. $l_p = 160$ mm according to the ACI code. As for the fiber elements, the transverse section is discretized by a grid of 2x2 mm fibers of concrete, which are replaced by steel when they are occupied by rebars. In addition, the hysteretic behavior of the concrete was defined through the parametric model proposed in [18], adapted to the constitutive model proposed in [19]. For steel rebars, the Giuffré-Menegotto-Pinto model with isoparametric strain hardening was used. The non-linear behavior of the plastic hinges is characterized by means of the moment-curvature backbone curve, i.e. M-φ, and the corresponding hysteretic law in each main direction. The M-φ curve is defined by yield moment, M_y, and the yield and ultimate curvatures, φ_y and φ_u. M_y was estimated using the empirical expression proposed by Fardis [9] with a reduction of 20% to account for the biaxial cyclic loading —interaction factor— [7,20]. First, φ_y and φ_u were calculated as $\varphi_y=\theta_y/l_p$ and $\varphi_u = \theta_u/l_p$, where θ_y and θ_u are the yielding and ultimate rotation obtained with empirical formulae [9]. Next, these initial values were modified to fit the results obtained from the tests. The stiffness degradation implemented in the hysteretic law was based on the study carried out by Rodriguez et al. [7].

The waffle-flat-plate is formed by a grid of ribs and solid zones around the columns. The grid of ribs, was modeled with elastic frame elements according to the transverse sections shown in Fig. 2c, with a 20% reduction of stiffness to account for cracking. The solid zones were modeled through shell elements with dimensions, on average, of 42x42 mm; these shell elements support geometry non-linearity. In order to reduce the computational time, non-linearity was adopted only for the shell elements of certain parts of the solid zones around the columns, those showing damage in the test. Shell elements were defined through multilayer shell sections with a total of nine layers. The thickness of each layer depends on the existence (or not) of

4

2i-0038

reinforcement. Rebars at the top and the bottom of the plate cross-section did not form a layer strictly speaking because they appeared as discrete points, for which reason they were considered as smeared steel layers of equivalent thicknesses, one per each reinforcement direction. Therefore, complete reinforcement entails four smeared steel layers, two for the upper part and two for the lower. The remaining layers are made up of concrete with variable thickness. The shell elements without reinforcement —plain concrete— do not have smeared steel layers. The solid zones were therefore subdivided into different parts according to the heterogeneous distribution of the reinforcement (Fig.4). The constitutive model used for concrete is based on the concept of damage mechanics and the smeared crack model. Cracks are assumed to form when the principal tensile stress exceeds the specified concrete tensile strength. After cracking, concrete is treated as an orthotropic material by smearing the cracks in the finite element. The properties of reinforcing steel are derived from the uniaxial materials for rebars in accordance with the corresponding angles of the steel layer in the model.
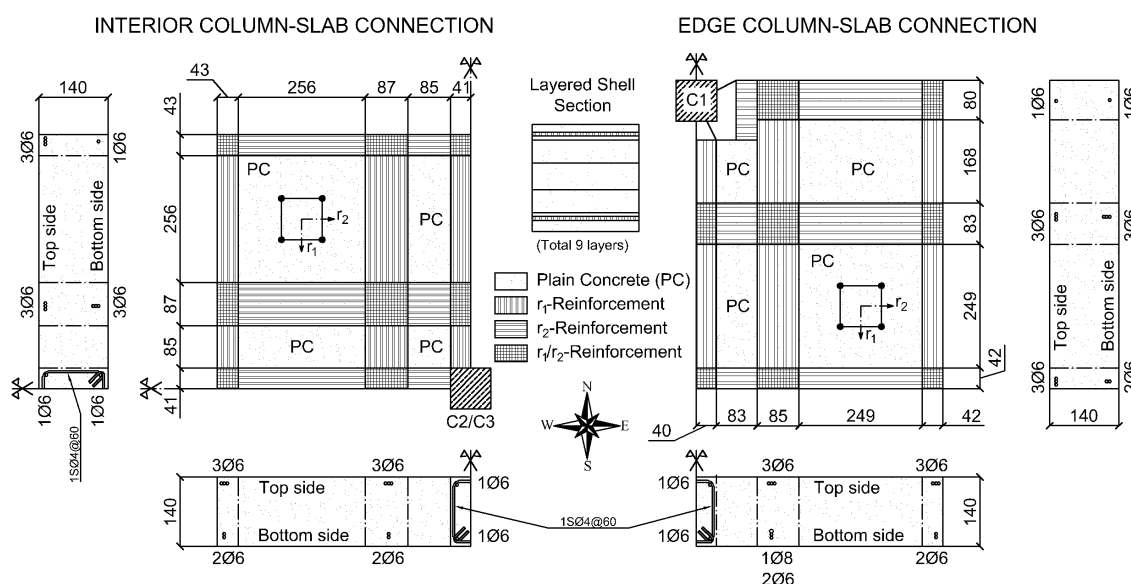
Fig. 4 – Solid zone discretization in interior and exterior column-slab connections

The spandrel beam (transverse beam) connected to the edge column C1 (Fig.2b) was modeled as an elastic beam element with torsional plastic hinges that reproduced the severe damage observed during the tests. The backbone curve of the torsional spring is a simplified version of the model developed by Valipour and Foster [21], shown in Fig.5. It is defined through three points: cracking torsion (φ_1, T_{cr}); ultimate torsional capacity (φ_2, T_u); and torsional failure (φ_3, T_u).
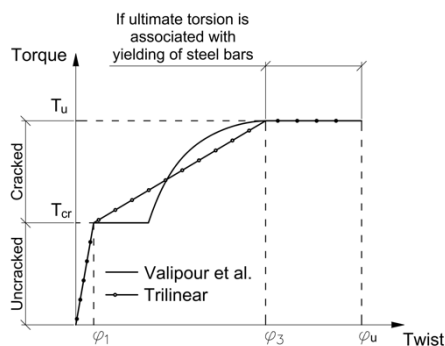
Fig. 5 – Constitutive model for torsion in a frame element

Finally, Fig.6 gives an overview of the numerical model that includes all the elements described above.

5
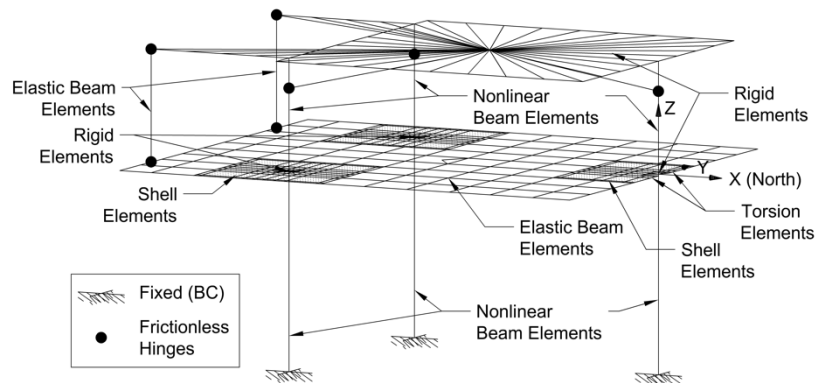
Fig. 6 – Overview of the model

2.3 Experimental validation of the benchmark numerical model

The benchmark numerical model was subjected to the same combination of loads as the specimen tested in laboratory using OpenSees software. Firstly, the gravity loads were applied in a static analysis; afterwards, non-linear time history analyses (NLTHAs) were carried out following the same sequence of seismic simulations used for the shake-table tests (from simulations T10 until C300). A mass-proportional damping model was defined and calibrated with experimental test data, in order to consider a classical damping matrix that prevents spurious damping [22] and to reproduce the increasing damping obtained in the tests. The damping matrix, $\mathbf{C}$ —classical— is defined by $\mathbf{C} = a_0\mathbf{M}$, where a_0 is a parameter and $\mathbf{M}$ is the mass matrix. In turn, a_0 is defined through the expression $a_0 = 2\xi_i\omega_i$, where ξ_i and ω_i are the damping ratio and the angular frequency —corresponding to the frequency, f_i— of the i-th vibration mode. The reference damping to calculate a_0 was $\xi_2 = 3\%$; this value is close to that obtained experimentally under elastic deformations, i.e. 2.4% [15]. Therefore, the parameter a_0 was obtained from $\xi_2 = 3\%$ and $\omega_2 = 2\pi f_2 = 2\pi 3.16 = 19.85$ rad/s, being equal to 1.19. Using this damping model, the damping ratio for the first vibration mode at failure was $\xi_1 = 7.2\%$ for $f_1 = 1.3$ Hz; this value is close to the one measured at the end of the tests, 9.2% [15].

Next, the response of the numerical model was compared with the experimental results. Fig.7 shows the history of the top displacement. The response in X and Y directions for the successive simulations —C35, C50, C100, C200i, C200 and C300— is depicted in the two central graphs of the figure. Further, some parts of these response histories, corresponding to specific simulations, are shown at the top and bottom of the figure. Simulations C50 and C200i are depicted for the X direction at the top —subfigures a) and b)— and simulations T10, C200i and C300 are depicted for the Y direction at the bottom part —subfigures c), d) and e). A good agreement is observed between the numerical prediction and experimental response, especially for the lower and moderate intensity levels, i.e. until the onset of C200. Nevertheless, for higher intensity levels —C200 and C300— the large strength degradation observed in the tests, especially at the ends of columns and at the edge of the column-slab connection, was not properly reproduced in the numerical model, which led to the observed differences. This is clearly seen in Fig.8, where the maximum displacements obtained for the two components in the numerical model are found to match the experimental results very well up to C200.

6
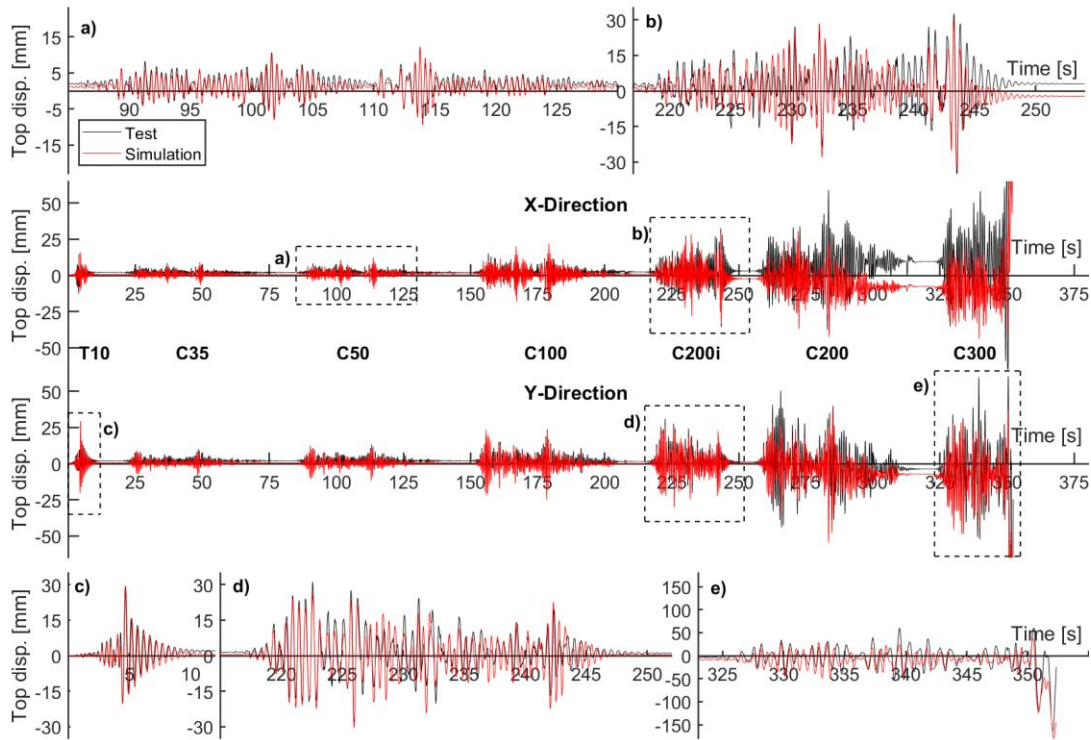
Fig. 7 – Top displacement history
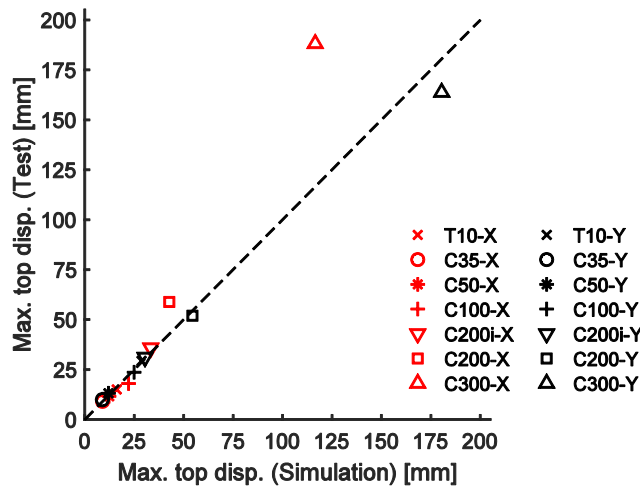
Fig. 8 –Maximum top displacement: numerical model vs experimental test

Fig.9 shows the history of total energy input in the specimen by the bidirectional seismic loading, E_I, (Fig.9a) and the input energy introduced separately by the X and Y components of ground motion, i.e, E_{Ix} (Fig. 9b) and E_{Iy} (Fig. 9c), respectively. The numerical model is seen to predict the input energy until the onset of simulation C200i very well. From this point on, the numerical model underestimates the input energy measured experimentally. It is important to note that the response history in terms of input energy provides a more convenient and accurate criterion to assess the goodness-of-fit between model and test, preferable to displacement or force histories. Displacements or forces are vectors defined at specific parts of the structure; in contrast, energy is a scalar quantity that characterizes the overall response of the entire structure [23]. Moreover, variations in the input energy history are better distinguished by using a logarithmic scale.

7
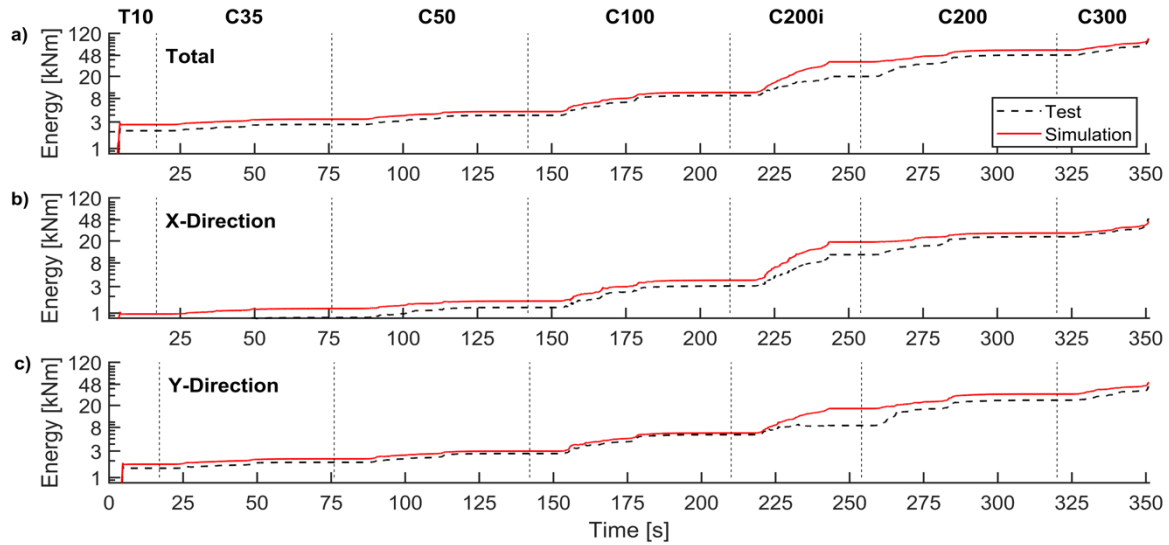
Fig. 9 – Input energy history

3. Seismic capacity of waffle-flat-plate structures

3.1 Numerical analyses

The benchmark numerical model described in the previous section was subjected to a selection of ground motion records to obtain the ultimate capacity of the specimen in terms of energy. The ground motion records were selected from the database prepared by Lucchini et al. [24]. In turn, this database was built from the international database of Campbell and Bozorgnia [25] by excluding all records with moment magnitude smaller than 5 and with a recognizable pulse in the ground velocity (i.e. pulse-like ground motion records were excluded). The records were selected on the basis of the following two criteria. First, the scale factor SF_{70} to be applied to the accelerograms in order to achieve a total input energy —in terms of pseudo velocity $V_E=(2E_I/M)^{0.5}$, where M is the total mass of the structure— of $V_E = 70$ cm/s was between 1/3 and 3. $V_E = 70$ cm/s is the input energy measured in the specimen tested on the shake-table (section 2.1) when it was on the brim of yield under uni- and bidirectional loadings [15,26]; it will be referred to as $V_{E,70}$ (=70 cm/s) herein. The energy input in the X and Y directions at the onset of yielding of the structure, i.e. when $V_{E,70}$ (=70 cm/s) is attained, will be respectively referred to as $E_{Ix,70}$ and $E_{Ix,70}$, and the corresponding equivalent velocities are $V_{Ex,70} = (2E_{Ix,70}/M)^{0.5}$ and $V_{Ey,70} = (2E_{Iy,70}/M)^{0.5}$. In general, $V_{Ex,70}$ and $V_{Ey,70}$ are different for each ground motion. Second, the PGA of the ground motion after scaling by SF_{70}, was 0.3g at most. This condition was imposed to avoid excessively large values of PGA when the numerical model collapses. The records were classified in five sets, Set 1 to Set 5, according the ratio $V_{Ey,70}/V_{Ex,70}$ as follows: $22.91°<atan(V_{Ey,70}/V_{Ex,70})<32.65°$ for Set 1; $32.65°<atan(V_{Ey,70}/V_{Ex,70})<42.40°$ for Set 2; $42.40°<atan(V_{Ey,70}/V_{Ex,70})<52.14°$ for Set 3; $52.14°<atan(V_{Ey,70}/V_{Ex,70})<61.88°$ for set 4; and $61.88°<atan(V_{Ey,70}/V_{Ex,70})<71.62°$ for Set 5. Seven records corresponding to different earthquakes were chosen within each set according to the lowest SF_{70} criteria. The records are identified by the earthquake name followed by the record sequence number in the Campbell and Bozorgnia database. The *X* and *Y* components of each ground motion scaled by SF_{70} were applied simultaneously to the benchmark numerical in successive seismic simulations by using a sequence of scaling factors 100%, 200%, 300%... until collapse. That is, 100% meant that the scaling factor applied to the original ground motion was SF_{70}, for 200% the scaling factor was $2 \times SF_{70}$, and so on. In addition, within each Set, one ground motion was selected and the *X* and *Y* components were applied separately to the numerical model until failure, in order to investigate the ultimate capacity under unidirectional seismic loads. In total, 45 NLTHAs were launched in a parallel scheme (OpenseesMP.exe) using a Dell Precision Tower 5810 with 12 cores at

8

3.60 GHz in order to minimize as much as possible the computational time. As a reference, the mean computational time required was 29 hours per core and record.

The elastic limit state and the ultimate limit state of the structure were determined on the basis of the top displacement at yielding δ_y and at collapse δ_u. The values of δ_y and δ_u were taken from the results of shake-table tests available in the literature involving waffle-flat-plate structures subjected to unidirectional [26], and bidirectional loading [15]. For unidirectional loadings, these values are $\delta_y = 19.7$mm and $\delta_u = 43$ mm [26]. For bidirectional loadings, the values adopted are $\delta_y = 25$ mm and $\delta_u = 55$ mm [15].

3.2 Results: capacity in terms of input energy and dissipated energy

The input energy on a structure subjected to bidirectional (horizontal) seismic loading can be expressed in terms of equivalent velocity V_E by $V_E = (V_{Ex}^2 + V_{Ey}^2)^{0.5}$. V_E can be interpreted as the modulus of a vector in the V_{Ex}-V_{Ey} plane. The same can be applied to the total energy that contributes to damage, E_D, defined as E_I minus the energy dissipated by inherent damping E_ξ, i.e. $E_D = E_I - E_\xi$. From the energy balance of the structure [4], it follows that E_D equals the sum of the elastic vibrational energy E_e and the energy dissipated through plastic deformations (hysteretic energy) E_h, i.e. $E_D = E_e + E_h$. For high levels of plastic deformations E_e becomes negligible in comparison with E_h [4], which leads to $E_D \approx E_h$. The energy that contributes to damage can be calculated independently in the X and Y directions, E_{Dx} and E_{Dy}, and is almost equal to the energy dissipated in the X and Y directions, E_{hx} and E_{hy}, i.e. $E_{Dx} \approx E_{hx}$ and $E_{Dy} \approx E_{hy}$. The corresponding equivalent velocities are $V_{Dx} = (2E_{Dx}/M)^{0.5}$, $V_{Dy} = (2E_{Dy}/M)^{0.5}$ and $V_D = (V_{Dx}^2 + V_{Dy}^2)^{0.5}$. Based on the above considerations, the values of V_D, V_{Dx} and V_{Dy} when the structure is near collapse can be interpreted as the ultimate energy dissipation capacity of the structure in the form of plastic deformations, expressed in terms of equivalent velocities.

Fig.10a shows V_E (defined by its components V_{Ex} and V_{Ey}) obtained through numerical simulations with the benchmark model described in section 2.2, subjected to the five sets of bidirectional ground motion records explained in section 3.1. The results of each set (Set 1 to Set 5) are identified in the figure with different colors. Also plotted in Fig.10a are the V_E´s obtained with the numerical model subjected to unidirectional ground motions (referred to as Set X and Set Y); they are identified in the legend with the letter X or Y added to the record name. Two limit states are represented in the Figure with a symbol for each record: (i) the yielding limit state —i.e. when the structure is on the brink of yield, which corresponds to lower values of input energy denoted hereafter by V_{Ee}; and (ii) the ultimate limit state —i.e. when the structure is near collapse, corresponding to higher values of input energy hereafter denoted by V_{Eu}. The two limit states are separated in the Figure by a solid black line. The mean $\bar{x}$ and mean plus/minus one standard deviation σ are also depicted with red and blue dashed lines, respectively, for V_{Ee} and V_{Eu}. The average values are $V_{Ee} = 96$ cm/s and $V_{Eu} = 226$ cm/s, with standard deviations equal to 23 cm/s and 63 cm/s, respectively. In terms of equivalent velocity this entails an ultimate energy dissipation capacity through plastic deformations of the structure over twice, i.e. 2.35, the energy the structure can store in the form of elastic deformations. In terms of energy, the increase is more than fivefold, i.e. 5.54. A more detailed analysis of the results is reported in Table 1, where the mean and the coefficient of variation, COV, are also shown for each set of records. Moderate differences are seen among the different groups for both V_{Ee} and V_{Eu}. The highest V_{Eu}/V_{Ee} ratios are found under unidirectional loading ($V_{Eu}/V_{Ee} = 2.63$ and $V_{Eu}/V_{Ee} = 2.67$ for X and Y directions, respectively), but they are still close to the mean 2.38 (COV = 0.22).

Moreover, Fig.10b shows the maximum energy dissipated through plastic deformations until failure (hysteretic energy) in terms of equivalent velocity, V_D, achieved in the numerical model under the aforementioned sets of ground motions. The same representation criteria as in Fig.10a are used. On average, $V_D = 142$ cm/s with a standard deviation of 42.57 cm/s. Table 1 indicates that the COV for V_{Eu} and V_D are 0.28 and 0.30, respectively. This means that the effect of bidirectional loading is not decisive for obtaining a reference value, on average, for the ultimate capacity of the structure in terms of energy.

+ MANJIL-1636	✳ HECTOR-1762	▽ HECTOR-1766	△ FRIULI-125	+ CHICHI-1490X	★ Benavent-Climent et al.(2019)	
○ CAPEMEND-826	× DUZCE-1619	◇ COALINGA-362	+ HECTOR-1794	○ KOBE-1115X	★ Benavent-Climent et al.(2015)	
✳ SFERN-68	▽ MORGAN-460	△ WHITTIER-673	○ CHICHI-1349	◇ LANDERS-888X	—— Elastic/Failure	
× SMADRE-1643	◇ IMPVALL-175	+ SUPERST-729	✳ CHALFANT-549	✳ CHALFANT-549X	– – $\overline{x}$	
▽ CHICHI-1435	△ LOMAP-799	○ ITALY-289	× LANDERS-854	× SMADRE-1643Y	– – $\overline{x} \pm \sigma$	
◇ IMPVALL-186	+ CHICHI-1534	✳ KOCAELI-1162	▽ NORTHR-1079	+ CHICHI-1490Y		
△ LANDERS-833	○ KOBE-1115	× HECTOR-1829	◇ CHICHI-1328	○ KOBE-1115Y		
+ CHICHI-1490	✳ NORTHR-986	▽ COALINGA-352	△ LOMAP-765	◇ LANDERS-888Y		
○ NORTHR-971	× LANDERS-850	◇ LANDERS-888	× SMADRE-1643X	✳ CHALFANT-549Y		
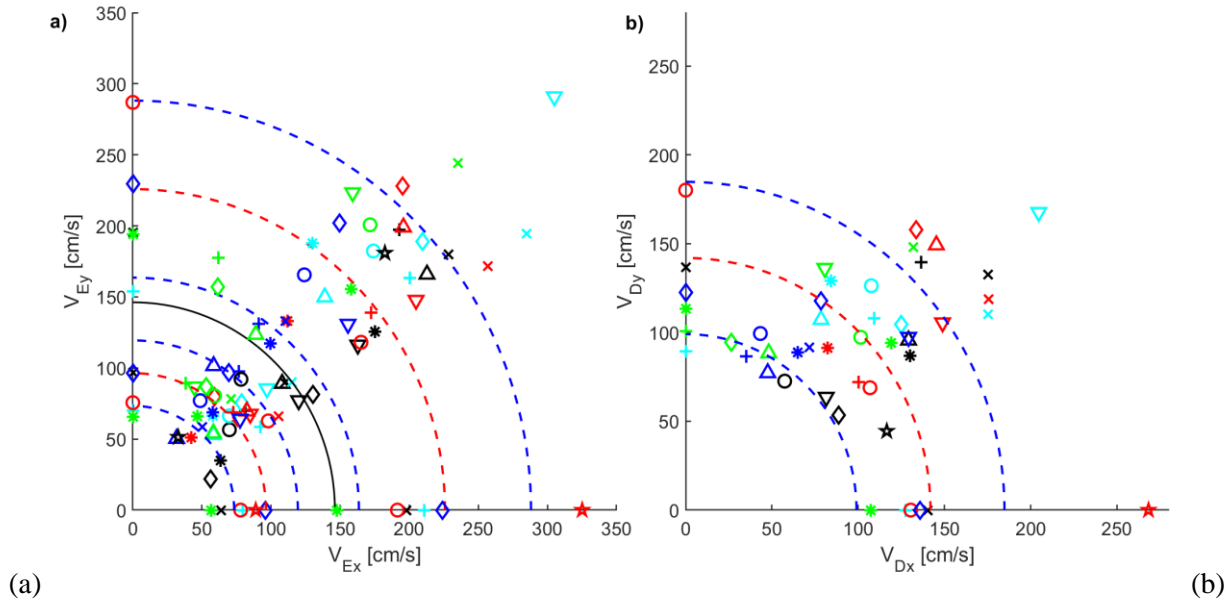
Fig. 10 – Bidirectional interaction diagram: (a) input energy; (b) hysteretic energy

Table 1 – Analysis of the input energy and the energy that contributes to damage obtained from NLTHAs

Set	mean V_{Ee} (cm/s)	COV V_{Ee} (cm/s)	mean V_{Eu} (cm/s)	COV V_{Eu} (cm/s)	mean V_{Eu}/V_{Ee}	COV V_{Eu}/V_{Ee}	mean V_D (cm/s)	COV V_D (cm/s)	mean V_D/V_{Eu}	COV V_D/V_{Eu}
X	74.72	0.18	194.35	0.13	2.63	0.10	128.22	0.09	0.67	0.08
1	107.79	0.30	218.10	0.28	2.12	0.27	147.35	0.31	0.68	0.12
2	108.12	0.20	284.60	0.24	2.63	0.11	177.23	0.23	0.63	0.05
3	103.24	0.17	248.53	0.19	2.43	0.15	169.00	0.23	0.68	0.09
4	94.50	0.22	180.69	0.22	1.94	0.16	117.39	0.20	0.66	0.15
5	94.57	0.10	229.73	0.27	2.42	0.22	134.30	0.27	0.59	0.11
Y	80.87	0.16	212.07	0.21	2.67	0.24	105.52	0.30	0.49	0.19
All	96.35	0.24	225.86	0.28	2.38	0.22	141.90	0.30	0.63	0.15

In Fig.10, the symbols located on the X or Y axis represent the responses of the models subjected only to one component (in X or Y direction, respectively) of the ground motion. For most records, the values of V_{Ee}, V_{Eu} and V_D obtained under unidirectional loadings were similar or slightly smaller than those obtained under bidirectional loadings (70%, 85% and 80%, respectively on average). One exception is the response under the Y component of Kobe-1115 —it alone that shows values of V_{Eu} and V_D that are about 40% higher than those under bidirectional seismic action. This behavior was also observed in the results of the shake-table tests: the V_{Eu} and V_D obtained for the specimen subjected to unidirectional loading along X direction [26] —represented by red star symbols— are 30% (Fig.10a) and 200% (Fig.10b) higher, respectively, than those achieved under

10

bidirectional loading [15] —represented by black star symbols— both of them being outside the range of values obtained in the numeric simulations —dashed blue lines in Fig.10. The limited results of this study therefore do not allow one to make a general statement about the higher capacity of structures under bidirectional loading than under unidirectional loads. Similar results were obtained by Rodriguez H. et al. in columns subjected to biaxial cyclic loadings and variable axial loads [7]. It is worth noting that the columns of the specimen are prone to undergo variable axial loads under both unidirectional and bidirectional cyclic loadings due to the structural scheme of the specimen itself —three columns. This could explain the results obtained. Interestingly, it can be observed in Fig.10 that the ultimate energy dissipation capacity of the structure tends to be quite balanced in the X and Y directions (i.e. the points in Fig.10a are close to the 45-degree line).

4. Conclusions

This study investigated the seismic behavior of reinforced concrete waffle-flat-plate structures subjected to bidirectional seismic loadings. The seismic behavior of a specimen that represents a 2/5 scale portion of a prototype structure of this type was tested on a shake-table under bidirectional ground motions until collapse. A non-linear finite element model —benchmark— that represented this specimen was developed, calibrated and validated with the experimental results. The numerical model was subjected to five sets of seven ground motion records. Each record was scaled with increasing values of the ground acceleration until collapse. In addition, five records were selected (one from each set) and the X and Y components were applied separately in only one direction until collapse. The results indicate that:

- The total input energy, V_{Eu}, or the total hysteretic energy, V_D —expressed in form of equivalent velocities— required to cause the collapse of the structure (ultimate capacity of the structure in terms of energy) remains basically the same when the two horizontal components of the ground motion are simultaneously applied.

- The total input energy that the structure can endure until collapse is about five times the maximum energy that the structure can store within the elastic range. In terms of equivalent velocity, the difference is about twice.

- The capacity of the structure under bidirectional loadings is in most cases slightly higher than under unidirectional loadings. Nevertheless, for some ground motions the response is opposite.

5. Acknowledgements

6. References

[1] CEN (2004): *European Standard EN 1998-1:2004 Eurocode 8: Design of structures for earthquake resistance, Part 1: General rules, seismic actions and rules for buildings*. Brussels: European Committee for Standardization.

[2] Priestley MJN, Calvi GM, Kowalsky MJ (2007): *Direct Displacement Based Seismic Design*. Pavia, Italy, IUSS Press.

[3] Sullivan TJ, Priestley MJN, Calvi GM (2012): *A Model Code for the Displacement-Based Seismic Design of Structures (DBD12)*. Pavia, Italy, IUSS Press.

[4] Akiyama H (1985): *Earthquake Resistant Limit-State Design for Buildings (English version)*. Tokyo, Japan: University of Tokyo Press.

[5] Bousias SN, Panagiotakos TB, Fardis MN (2002): Modelling of RC members under cyclic biaxial flexure and axial force. *Journal of Earthquake Engineering*, **6** (2), 213-238.

[6] Rodrigues H, Varum H, Arêde A, Costa A (2012). A comparative analysis of energy dissipation and equivalent viscous damping of RC columns subjected to uniaxial and biaxial loading. *Engineering Structures*, **35,** 149-164.

[7] Rodrigues H, Furtado A, Arêde A (2016): Behavior of Rectangular Reinforced-Concrete Columns under Biaxial Cyclic Loading and Variable Axial Loads. *Journal of Structural Engineering*, **142** (1), 1-8.

11

[8] De Stefano M, Faella G (1996): An evaluation of the inelastic response of systems under biaxial seismic excitations. *Engineering Structures*, **18** (9), 724-731.

[9] Fardis M (2009): *Seismic design, assessment and retrofitting of concrete buildings: based on EN-Eurocode 8. vol. 8*. Springer Verlag.

[10] Rodrigues H, Arêde A, Varum H, Costa A (2013): Damage evolution in reinforced concrete columns subjected to biaxial loading. *Bulletin of Earthquake Engineering*, **11** (5), 1517-1540.

[11] Magliulo G, Ramasco R (2007): Seismic response of three-dimensional r / c multi-storey frame building under uni- and bi-directional input ground motion. *Earthquake Engineering and Structural Dynamics*, **36** (May), 1641-1657.

[12] Sebastiani PE, Liberatore L, Lucchini A, Mollaioli F (2018): A new method to predict the critical incidence angle for buildings under near - fault motions. *Structural Engineering and Mechanics*, **68** (5), 575-589.

[13] Dutta SC, Kunnath SK (2013): Effect of bidirectional interaction on seismic demand of structures. *Soil Dynamics and Earthquake Engineering*, **52**, 27-39.

[14] Goel RK (1997): Seismic response of asymmetric systems: Energy-based approach. *Journal of Structural Engineering*, **123** (11), 1444-1453.

[15] Benavent-Climent A, Galé-Lamuela D, Donaire-Avila J (2019): Energy capacity and seismic performance of RC waffle-flat plate structures under two components of far-field ground motions: Shake table tests. *Earthquake Engineering & Structural Dynamics*, **48** (8), 949-969.

[16] Li C, Bi K, Hao H (2019): Seismic performances of precast segmental column under bidirectional earthquake motions: Shake table test and numerical evaluation. *Engineering Structures*, **187** (January): 314-328.

[17] Mckenna FT (1997): *Object-oriented finite element programming: Frameworks for analysis, algorithms and parallel computing*. University of California, Berkeley.

[18] Mohd YM (1994): *Nonlinear analysis of prestressed concrete structures under monotonic and cyclic loads*. University of California, Berkeley.

[19] Maekawa K, Pimanmas A, Okamura H (2003): *Non Linear Mechanics of Reinforced Concrete*. New York, USA: Spon Press.

[20] Rodrigues H, Varum H, Arêde A, Costa AG (2013): Behaviour of reinforced concrete column under biaxial cyclic loading—state of the art. *International Journal of Advanced Structural Engineering*, **5** (1), 1-12.

[21] Valipour HR, Foster SJ (2010): Nonlinear reinforced concrete frame element with torsion. *Engineering Structures*, **32** (4), 988-1002.

[22] Charney FA (2008): Unintended Consequences of Modeling Damping in Structures. *Journal of Structural Engineering*, **134** (4), 581-592.

[23] Fardis MN (2018): From force- to displacement-based seismic desing of concrete structures and beyond. *16ᵗʰ European Coinference on Earthquake Engineering*, Thessaloniki, Greece.

[24] Lucchini A, Franchin P, Mollaioli F (2017): Uniform hazard floor acceleration spectra for linear structures. *Earthquake Engineering & Structural Dynamics*, **46** (7), 1121-1140.

[25] Campbell KW, Bozorgnia Y (2007): Campbell-Bozorgnia NGA Ground Motion Relations for the Geometric Mean Horizontal Component of Peak and Spectral Ground Motion Parameters. *Technical Report PEER*, Pacific Earthquake Engineering Research Center, University of California, Berkeley, USA.

[26] Benavent-Climent A, Donaire-Avila J, Oliver-Saiz E (2016): Shaking table tests of a reinforced concrete waffle-flat plate structure designed following modern codes: Seismic performance and damage evaluation. *Earthquake Engineering & Structural Dynamics*, **45** (2), 315-336.